

Temperature dependent orbital degree of freedom in a bilayer manganite by magnetic Compton scattering

Yinwan Li^{1,2}, P. A. Montano^{1,3}, J.F. Mitchell², B. Barbiellini⁴, P. E. Mijnen^{4,5}, S. Kaprzyk^{4,6} and A. Bansil⁴

¹*Department of Physics, University of Illinois, Chicago IL 60680*

²*Materials Science Division, Argonne National Laboratory, Argonne IL 60439*

³*Materials Sciences and Engineering, U.S. Department of Energy, 1000 Independence Avenue, Washington DC 20585-1290*

⁴*Physics Department, Northeastern University, Boston MA 02115*

⁵*Interfaculty Reactor Institute, Delft University of Technology, 2629 JB Delft, The Netherlands*

⁶*Academy of Mining and Metallurgy AGH, 30059 Kraków, Poland*

(Dated: November 19, 2018)

We have measured temperature-dependent magnetic Compton profiles (MCPs) from a single crystal of $\text{La}_{1.2}\text{Sr}_{1.8}\text{Mn}_2\text{O}_7$. The MCPs, which involved the scattering of circularly polarized x-rays, are in general related to the momentum density of *all* the unpaired spins in the system. Nevertheless, we show that when the x-ray scattering vector lies along the [110] direction, the number of magnetic electrons of a *specific* symmetry, i.e. *d*-electrons of $x^2 - y^2$ symmetry, yield a distinct signature in the MCP, allowing us to monitor substantial changes in the occupancy of the $d_{x^2-y^2}$ states over the investigated temperature range of 5-200K. This study indicates that magnetic Compton scattering can provide a powerful window on the properties of specific magnetic electrons in complex materials.

PACS numbers: 73.22.Dj, 75.75+a, 75.10-b

Layered manganites $((\text{La}_{1-x}\text{Sr}_x\text{MnO}_3)_n\text{SrO})$ have been the subject of great current interest not only because they exhibit the colossal magnetoresistance (CMR) effect [1, 2], but also because these systems display a wide variety of magnetic properties [3] and undergo phase transitions associated with changes in the orbital degrees of freedom. Here we consider the application of the x-ray scattering spectroscopy in the deeply inelastic or so-called Compton scattering regime (i.e. involving a large transfer of energy and momentum in the scattering process) in order to gain a handle on the properties of magnetic electrons in the manganites.

The scattering cross-section from magnetic electrons is typically several orders of magnitude smaller than in the more conventional charge scattering channel, and therefore, magnetic Compton scattering experiments have become feasible on complex materials only in the last few years via the use of circularly polarized light at the high energy, high intensity synchrotron sources [4]. Previous magnetic Compton scattering work on the manganites, which has been limited to the double layer La-manganite, has focused on the case where the x-ray scattering vector lies along the [100] or the [001] crystal direction [5, 6, 7, 8]. The shape of the associated [100] and [001] MCPs, however, is dominated by the *d* electrons of t_{2g} (i.e. *xy*, *yz* and *zx*) symmetry. However, t_{2g} levels lie ~ 1 eV below the Fermi energy and are thus relatively 'inert'—more central to the understanding of the manganites is the behavior of the magnetic states of e_g (i.e. $x^2 - y^2$ or $3z^2 - r^2$) symmetry.

This article focuses on the case where the x-ray scattering vector is chosen to lie along the [110] crystal direction. We show that the resulting [110] MCP, when Fourier-transformed to real space, contains a remarkable signa-

ture of the number of $d_{x^2-y^2}$ electrons through the presence of a well-defined dip around 1 Å. Along the [110] direction, the shapes of various magnetic orbitals conspire in such a way as to render the depth of the aforementioned dip quite insensitive to the presence of other orbitals (t_{2g} and $d_{3z^2-r^2}$). [110] MCPs in $\text{La}_{1.2}\text{Sr}_{1.8}\text{Mn}_2\text{O}_7$ over the temperature range of 5K-200K are presented. In order to help interpret these experimental results, we also present the first all-electron computations of the MCP in the closely related compound $\text{LaSr}_2\text{Mn}_2\text{O}_7$. From our analysis of the temperature dependent MCP's, we adduce that the number of $d_{x^2-y^2}$ states increases from about 0.3 for each Mn atom at 5K to around 0.44 at 160K, but then decreases rapidly to the low-*T* value of ~ 0.3 by 200K, suggesting that the system has undergone significant changes in the electronic structure. We emphasize that the 7T magnetic field present during the experiments makes the samples electronically homogeneous and that this field is sufficiently strong to collapse polarons [9].

The magnetic Compton profile, $J_{mag}(p_z)$, for momentum transfer along the scattering vector p_z is defined by

$$J_{mag}(p_z) = J_{\uparrow}(p_z) - J_{\downarrow}(p_z), \quad (1)$$

where J_{\uparrow} (J_{\downarrow}) is the majority(minority) spin Compton profile. J_{mag} can be expressed in terms of a double integral of the spin density, $\Delta\rho(\mathbf{p})$:

$$J_{mag}(p_z) = \int \int \Delta\rho(\mathbf{p}) dp_x dp_y, \quad (2)$$

where $\Delta\rho(\mathbf{p}) \equiv \rho_{\uparrow}(\mathbf{p}) - \rho_{\downarrow}(\mathbf{p})$.

MCP measurements were carried out using the elliptical multipole wiggler at beamline 11-B at the Advanced

Photon Source [10] on a high quality single crystal of $\text{La}_{1.2}\text{Sr}_{1.8}\text{Mn}_2\text{O}_7$ using circularly polarized photons. The sample is $10 \times 5 \times 2 \text{ mm}^3$, where the shortest side is along the crystal c -axis. The sample was fixed to the holder with a specially made Al clip to avoid magnetic contamination. The MCP's were obtained using magnetic fields of 3T and 7T along the three high symmetry directions [001], [100], and [110] for four different temperatures in each case: 5K, which is well below the Curie temperature $T_c = 129\text{K}$, and at 100K, 160K, and 200K, the last temperature being well above T_c . The momentum resolution was $\sim 0.4 \text{ a.u.}$ $J_\uparrow(p_z)$ and $J_\downarrow(p_z)$ were measured by flipping the photon polarization. In this article, we focus on the [110] MCP and its temperature dependence under a 7T field. We have also measured the MCP along [100] and [001] and observed no significant variation in shape with temperature [5, 6].

The electronic structure, magnetic momentum density, and the MCPs along principal symmetry directions were computed within an all-electron, fully charge and spin self-consistent semi-relativistic KKR framework [11] for $\text{LaSr}_2\text{Mn}_2\text{O}_7$ in the I4/mmm (No. 139) crystal structure [12]. All computations were carried out to a high degree of accuracy, e.g. the potentials were converged to better than 10^{-5} Ry . The momentum density was computed over a fine mesh of 129.6×10^6 points within a sphere of radius 14.9 a.u. in \mathbf{p} space [13]. This data set was used to evaluate various spin-polarized projections and the MCP's.

Our computed electronic structure (for $x = 0.5$) is in good overall accord with two relevant earlier studies [14, 15]. All calculations agree on a nearly or wholly halfmetallic ferromagnetic band structure with the Fermi level crossing Mn d bands. The (\uparrow)-spin bands are metallic with a Fermi surface (FS) consisting of three sheets. The (\downarrow)-spin FS sheet has the shape of a pillar. We obtain a spin-only magnetic moment of $3.178 \mu_B$ on each Mn atom, in line with our experimental values of $3.4 \mu_B$ at 7T and $3.1 \mu_B$ at 3T, and of $3.0 \mu_B$ for $x = 0.4$ [16]. Most other atoms are found to carry small moments of a few times $10^{-2} \mu_B$. The total moment per formula unit is found to be $6.976 \mu_B$, slightly lower than the values of $6.995 \mu_B$ [14] and $7.0 \mu_B$ [15] in earlier studies.

The interpretation of the momentum density and the MCP's is aided by Fig. 1, which shows two typical 2D-projections (upper frames) of the *magnetic* momentum density $\Delta\rho(\mathbf{p})$, as well as two orthogonal cuts through the origin of $\Delta\rho(\mathbf{p})$ (lower frames). The (001) projection in Fig. 1(a), for instance, shows that the FS—seen by the presence of large and smaller squarish features—is essentially 2D in character. Underlying these FS features, the uncompensated magnetic contribution yields a strong peak at $(p_x, p_y) \sim (1.1, 1.1) \text{ a.u.}$ in the projection of (a). We have analyzed the origin of this peak extensively by considering a series of cuts through $\Delta\rho(\mathbf{p})$ parallel to various high symmetry directions to establish

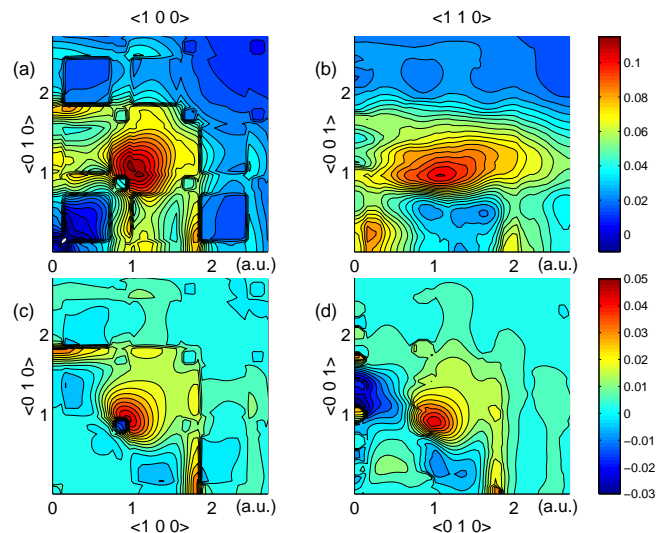


FIG. 1: Theoretical 2D-projection (i.e. 1D-integral) of the magnetic momentum density $\Delta\rho(\mathbf{p})$ onto: (a) (001), and (b) (110) planes. (c) and (d) give 2D-cuts through the 3D-density $\Delta\rho(\mathbf{p})$ in the $(p_z = 0)$ and $(p_x = 0)$ planes, respectively.

that this feature arises from wavefunctions of t_{2g} symmetry. Indeed, the (001) and the (100) cuts in (c) and (d), respectively, both show a peak lying along the diagonal line as expected for an xy or yz type orbital.

Recalling from Eq. (2) that the MCP involves a double integral or equivalently a 1D-projection of $\Delta\rho(\mathbf{p})$, the form of the MCP's for momentum transfer along the principal symmetry directions can be understood straightforwardly from the 2D-projections of Figs. 1 (a) and (b). For example, the [100] MCP represents a further projection of the distribution of (a) on the horizontal [100]-axis, so that it contains a t_{2g} related peak around 1.1 a.u., which is also the case for the [001] MCP (as seen by projecting (b) on the vertical axis). Such a peak is observed in our [100] and [001] MCP's and in those of Ref. 7. These MCP's however are not shown here since our focus in this article is on the [110] MCP. We see from (b) that the region of high density is elongated along [110], so that the resulting [110] MCP (Fig. 2) is relatively flat unlike the [100] or the [001] MCP's, particularly after the experimental resolution is included. Fig. 2 shows a remarkable level of agreement between theory and experiment, some discrepancies notwithstanding [17]. The structures in the unbroadened theory MCP (thin solid line) are due partly to the FS, but are washed out under the resolution of the present experiment (0.4 a.u.). Higher resolution measurements would be most interesting in gaining insight into FS signatures in the momentum density.

Fig. 3 presents the temperature dependence of the [110] MCP. By invoking a molecular orbital picture [7], substantial changes observed in the shape of the [110] MCP with temperature can be understood. Although such an

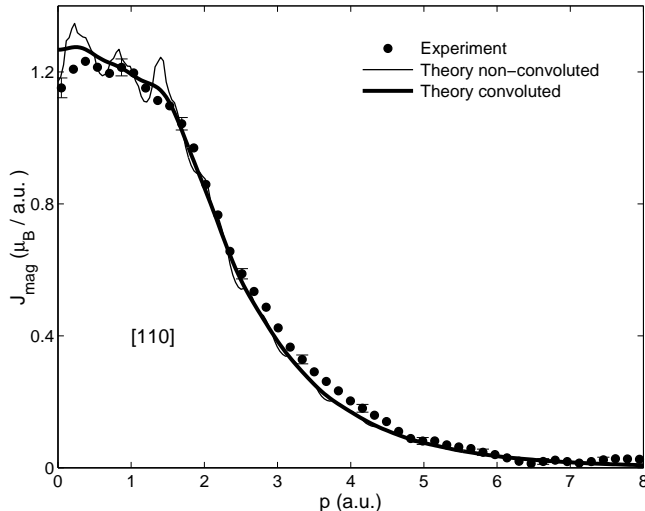


FIG. 2: Comparison of the theoretical and experimental [110] MCP, the latter taken at 5K under a 7T magnetic field along [110]. Theoretical curves are shown with (thick line) and without (thin line) the effect of experimental resolution of 0.4 a.u. (FWHM). All curves are normalized such that the area gives the measured magnetic moment of $3.4\mu_B/\text{Mn}$ atom.

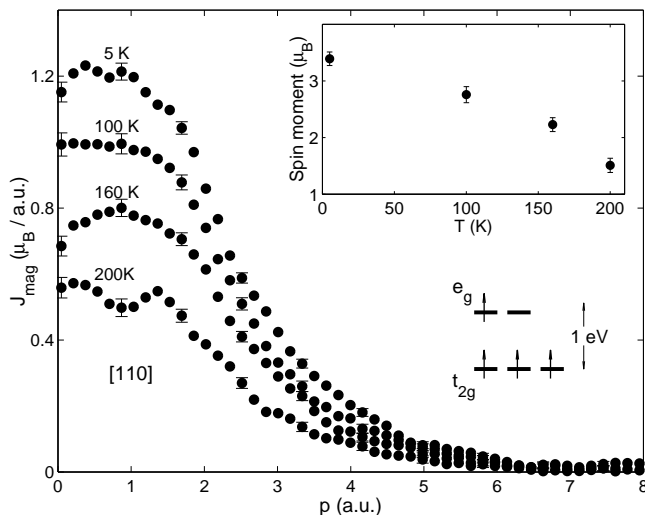


FIG. 3: Temperature dependence of the [110] MCP under an external magnetic field of 7T. Upper inset gives the corresponding spin magnetic moments. A representative energy level diagram of the relevant magnetic levels derived from our band structure computations is given in the lower inset.

analysis is not rigorous, it nevertheless provides a handle on the important question of orbital occupancies. Assuming thus that the 3.6 Mn electrons essentially retain their atomic character, one expects these to go into the up-spin states in accord with Hund's first rule (see lower inset in Fig. 3), with three electrons occupying the up-

spin t_{2g} orbitals (d_{xy}, d_{xz}, d_{yz}) and the remaining 0.6 electrons the ($d_{x^2-y^2}, d_{3z^2-r^2}$) orbitals. The total spin moment of course decreases with temperature following the Curie-Weiss law as seen from the upper inset in Fig. 3. Note that the spin moment does not show anomalies observed at lower field [18], confirming that the phase is electronically homogeneous under the field of 7T used in this work.

The energy level diagram in Fig. 3 makes it clear that the occupancy of the t_{2g} orbitals, which lie about 1 eV below E_F —well above kT —will change little with T , and that the variation with T will occur mainly through the redistribution of 0.6 e_g electrons between the $d_{x^2-y^2}$ and $d_{3z^2-r^2}$ orbitals. For this purpose, we consider the reciprocal form factor, $B(\mathbf{r})$, which is defined as the Fourier transform of the spin momentum density [19]

$$B(\mathbf{r}) = \int \Delta\rho(\mathbf{p}) \exp(-i\mathbf{p} \cdot \mathbf{r}) d\mathbf{p}. \quad (3)$$

We now express $\Delta\rho(\mathbf{p})$ as a sum over the momentum density of the molecular orbitals $\psi_i^{MO}(\mathbf{p})$ of the magnetic electrons, weighted by their occupancies n_i :

$$\Delta\rho(\mathbf{p}) = \sum_i n_i |\psi_i^{MO}(\mathbf{p})|^2. \quad (4)$$

By transforming Eq. (4) into real space, it is easily shown that $B(\mathbf{r})$ gives the autocorrelation of the magnetic orbitals, $\psi_i^{MO}(\mathbf{r})$

$$B(\mathbf{r}) = \sum_i n_i \int \psi_i^{MO}(\mathbf{s}) \psi_i^{*MO}(\mathbf{s} + \mathbf{r}) d\mathbf{s} \quad (5)$$

where the integrals are the standard two-center overlap functions. Alternately, $B(\mathbf{r})$ along a given direction can be obtained directly by taking the 1D-Fourier transform of the MCP along that direction by comparing Eqs. (2) and (3).

Fig. 4 presents the $B(\mathbf{r})$ results along [110] obtained from the MCP's of Figs. 2 and 3. Notable features are the presence of a dip at $r \approx 1 \text{ \AA}$ and oscillations at higher distances. As expected, the shape of the theory curve is in very good accord with the 5K experimental data. Systematic changes in shape with temperature can be interpreted by recalling that $B(\mathbf{r})$ gives the autocorrelation of the magnetic orbitals. We consider the dip in $B(\mathbf{r})$ first. We have computed the overlap integral in Eq. (5) for the t_{2g} and e_g orbitals using Slater type orbitals (STO). The key observation that emerges is that the large dip in $B(\mathbf{r})$ along [110] is produced essentially by the autocorrelation of the $d_{x^2-y^2}$ orbital. This can be understood qualitatively from the schematic picture of a $d_{x^2-y^2}$ orbital in Fig. 4. It is obvious that when this orbital is translated along [110], the positive and negative lobes will overlap and yield a *negative* dip at a distance of the order of orbital dimensions. In contrast, the d_{xy} and $d_{3z^2-r^2}$ orbitals give positive contributions near 1 \AA ; there also are

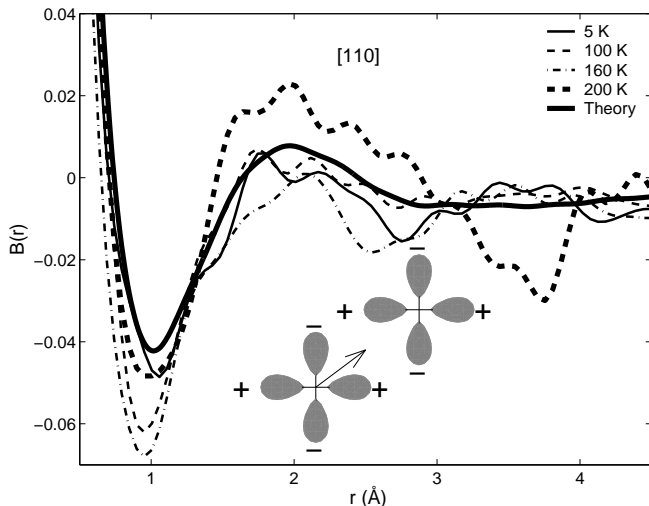


FIG. 4: $B(r)$ results for r along $[110]$ obtained from the experimental and the broadened theoretical MCP's of Fig. 2, and the MCP's at different temperatures of Fig. 3. [20] Inset: Schematic diagram of a $d_{x^2-y^2}$ orbital centered at the origin with lobes along $[100]$ and $[010]$ and the same orbital displaced along $[110]$.

small negative contributions from d_{xz} and d_{yz} orbitals. These results indicate that the size of the negative dip in $B(r)$ is correlated with the $d_{x^2-y^2}$ occupancy. Computations in which all magnetic orbitals are included show that one can fit the minimum value, B_{min} , of $B(r)$ along $[110]$ by a linear equation involving the occupancy f of the $d_{x^2-y^2}$ orbital: $B_{min} = af + b$, where $a = -0.130$ and $b = 0.004$ [20]. Using this fit, the T dependent data of Fig. 4 gives f values of 0.38, 0.48, 0.53 and 0.38, corresponding to 5, 100, 160 and 200K. Thus, at low T , the $d_{3z^2-r^2}$ occupancy is 0.22. By 160K, this number decreases to 0.07, but then increases relatively rapidly to the low- T value by 200K. These variations correlate remarkably well with those in the apical oxygen distance, D_{apical} , in the MnO_6 octahedra. Ref. [16] reports that D_{apical} decreases up to ≈ 120 K, but then begins to increase quite rapidly. A decrease in D_{apical} is expected to raise the energy of the $d_{3z^2-r^2}$ levels and to reduce their occupancy or, equivalently, to increase the $d_{x^2-y^2}$ population, consistent with earlier observations.

Turning to the behavior of $B(r)$ beyond the dip, Fig. 4 shows that for $r \gtrsim 1.5$ Å there is little overall change in shape up to 160K. The 200K curve however displays striking differences in that the broad feature around 2Å develops a significantly larger amplitude accompanied by the appearance of a new dip at ≈ 3.5 Å. We emphasize that sizable values of $B(r)$ beyond atomic dimensions are a hallmark of electronic states extending over larger distances as a result of the mixing of Mn and O orbitals in the MnO_2 planes. The fact that at 200K $B(r)$ exhibits

a dramatic change in shape in that the dip reverts to the low- T value and strong oscillations appear at higher distances, indicates that the system has undergone some orbital modification in which the oxygen wavefunction character plays an important role. We should keep in mind, however, that, at the doping level of our sample, the system lies near a multi-critical point in the phase diagram, so that pin-pointing the detailed nature of the aforementioned orbital change will generally be difficult.

In conclusion, our study shows that magnetic Compton scattering spectra taken under a field of 7T allow access to the properties of the electronically homogeneous phase of the manganite over a wide range of temperatures. This strong magnetic field also collapses polarons. The shape of the spectrum for momentum transfer along the $[110]$ direction contains a remarkable signature of the occupancy of the $d_{x^2-y^2}$ electrons. These results indicate that magnetic Compton scattering can provide a powerful new spectroscopic window for investigating orbital physics and magnetic electrons in complex materials.

We acknowledge important discussions with Robert Markiewicz. This work is supported by the US Department of Energy contract DE-AC03-76SF00098, and benefited from the allocation of supercomputer time at NERSC, Northeastern University's Advanced Scientific Computation Center (ASCC), and the Stichting NCF (Foundation National Computer Facilities).

-
- [1] N. Mathur and P. Littlewood, *Physics Today*, January 2003, p. 25; Y. Tokura, *Physics Today*, July 2003, p. 50.
 - [2] Y. Moritomo *et al.*, *Nature* **380**, 141 (1996).
 - [3] M. Kubota *et al.*, *J. Phys. Chem. Solids* **60**, 1161 (1999).
 - [4] J.E. McCarthy *et al.*, *J. Synchrotron Rad.* **4**, 102 (1997).
 - [5] Y. Li *et al.*, *Bull. Am. Phys. Soc.* **46**, 167 (2001).
 - [6] P.A. Montano *et al.*, *Bull. Am. Phys. Soc.* **48**, 193 (2003).
 - [7] A. Koizumi *et al.*, *Phys. Rev. Lett.* **86**, 5589 (2001).
 - [8] A. Koizumi *et al.*, *Phys. Rev. B* **69**, 060401(R) (2004).
 - [9] L. Vasiliu-Doloc *et al.*, *Phys. Rev. Lett.* **83**, 4393 (1999).
 - [10] P.A. Montano *et al.*, *Proc. SPIE* **3773**, 262 (1999).
 - [11] A. Bansil *et al.*, *Phys. Rev. B* **60**, 13 396 (1999).
 - [12] R. Seshadri *et al.*, *Solid State Commun.* **101**, 453 (1997).
 - [13] P.E. Mijnarends and A. Bansil, in *Positron Spectroscopy of Solids*, eds. A. Dupasquier and A.P. Mills (IOS Press, Amsterdam, 1995), p. 25.
 - [14] P.K. de Boer and R.A. de Groot, *Phys. Rev. B* **60**, 10 758 (1999).
 - [15] X.Y. Huang *et al.*, *Phys. Rev. B* **62**, 13 318 (2000).
 - [16] J.F. Mitchell *et al.*, *Phys. Rev. B* **55**, 63 (1997).
 - [17] Our computations do not include correlation corrections, see e.g. B. Barbiellini and A. Bansil, *J. Phys. Chem. Solids* **62**, 2181 (2001).
 - [18] M. Kubota *et al.*, *J. Phys. Soc. Jpn.* **69**, 1986 (2000).
 - [19] B. Barbiellini and A. Shukla, *Phys. Rev. B* **66**, 235101 (2002).
 - [20] The formula for B_{min} was obtained by choosing STOs and an occupancy of 3 for the t_{2g} states, of f for the $d_{x^2-y^2}$ and $(0.6 - f)$ for the $d_{3z^2-r^2}$ states. The STOs

yield $B(r) = (1 + t + c_2 t^2 + \dots + c_6 t^6) \exp(-t)$, where $t = Z_{eff} r/3$, Z_{eff} is the effective charge of the atomic potential and the coefficients c_i depend on f (see, e.g., calculations of overlap integrals by M.P. Barnett, *Int.*

J. Quant. Chem. **95**, 791 (2003)). In order to analyze changes in shape, all curves in Fig. 4 are normalized such that, $B(0) = 1$.